



Analytical and Experimental Investigation into Increasing Operating Bandwidth of Piezoelectric Energy Harvesters

R. Hosseini^{1*}, M. Hamed¹, H. Golparvar², O. Zargar¹

¹ School of Mechanical Engineering, College of Engineering, University of Tehran, Tehran, Iran

² Faculty of Aerospace Engineering, K. N. Toosi University of Technology, Tehran, Iran

ABSTRACT: Piezoelectric cantilevers are mostly used for vibration energy harvesting. Changing the shape of the cantilevers could affect the generated output power and voltage. In this work, vibration energy harvesting via piezoelectric resonant unimorph cantilevers is considered. Moreover, a new design to obtain more wideband piezoelectric energy harvester is suggested. This study also provides a comprehensive analysis of the output voltage relationships and deducing an essential precise rule of thumb to calculate resonance frequency in cantilever-type unimorph piezoelectric energy harvesters using the Rayleigh-Ritz method. The analytical formula is then analyzed and verified by experiment on a fabricated prototype. The analytical data was found in an agreement with the experimental results. An important finding is that among all the unimorph tapered cantilever beams with uniform thickness, the triangular cantilever, can lead to highest resonance frequency and by increasing the ratio of the trapezoidal bases, the resonance frequency decreases. It is concluded that the shape can have a significant effect on the output voltage and therefore maximum output power density. Some triangular cantilever energy harvesters can arrange in pizza form using cantilever arrays. This arrangement decreases the occupied space and can lead to increasing the power density and also operating bandwidth.

Review History:

Received: 1 April 2018

Revised: 10 October 2018

Accepted: 22 November 2018

Available Online: 21 December 2018

Keywords:

Vibration energy harvesting

Resonant frequency

Cantilever arrays

Wideband operation

Power density

1- Introduction

A vibration powered generator is a type of electric generator that converts the kinetic energy from vibration into electrical energy. The vibration may be from seismic (ground) vibrations, acoustic pressure waves, forces applied directly to the load on the working surface or other surrounding sources [1-6]. The conversion of ambient energy in the environment surroundings into electrical energy is called energy harvesting or energy scavenging. During the past decade, energy harvesting from mechanical vibrations of ambient environments has attracted the attention of many researchers due to the ever-increasing desire to produce wireless and portable electronics with extended life [7,8]. While sensors and wireless electronic equipment are becoming more prevalent, delivering power to the wireless sensor networks is difficult and remains a challenge. Mechanical vibrations are more considered to study in recent decades [9,10]. They are abundant and ubiquitous in the environment, and they provide no limitations in their applications on cloudy days or at nights. The standard mechanisms for vibration energy harvesting are; using electrostatic devices, electromagnetic field, and utilizing piezoelectric materials [6,11]. Piezoelectric based material's flexibility in volume and size has led to the development of micro-generators, that they are utilized in places where other sources of energy are not readily available [6,12-16].

Vibration energy harvesting with the piezoelectric material can currently generate up to 300 microwatts per cubic centimeter, making it an attractive method of powering low-power electronics [17]. Compared to other structural forms

of beams [18], a cantilever has the maximum deformation under the same conditions. The larger deflection leads to higher strain and more output power. Therefore the vast majority of piezoelectric vibration power scavenging devices use a cantilever structure [19-22]. A cantilever-type power scavenger, as well as a tapered one, considered the optimum design had been intensively studied [23-25]. It is observed that the tapered one ensures a large constant and more uniform distribution of strain in the piezoelectric layer resulting in higher power output in comparison to the rectangular beam [6].

A piezoelectric unimorph cantilever structure includes one inactive (substrate) and one active (piezoelectric) layer, whereas a bimorph cantilever has one inactive layer, but two active layers. In order to analyze and calculate the resonance frequency of unimorph trapezoidal V-shaped cantilever beams (in particular case triangular cantilevers), a significant and straightforward analytical formula using Rayleigh-Ritz method is derived. Furthermore, the optimization method for adjusting (enhancing or lowering) the resonance frequency with this formula is used. In the particular case that piezoelectric layer thickness is negligible, the resonance frequency formulation for a simple triangular cantilever is formulated that is by that extracted in [26-28]. It is noteworthy that a cantilever beam has many different modes of vibration in different resonance frequencies. The fundamental mode of vibration typically provides the most deflection and hence output voltage and power. Accordingly, power scavengers are generally designed to operate in the fundamental resonance frequency [15,16].

In this research, under the influence of base excitation,

Corresponding author, E-mail: R.Hosseini.mech@gmail.com

estimation of voltage response for rectangular and tapered unimorph piezoelectric cantilever beam is done. Analytical formulas in forced vibration analysis are validated by experimental results. Studies are carried out using MATLAB and MATHEMATICA software. Some parts of the code are written in MATHEMATICA, and the output is used in the MATLAB [6].

This paper presents a work on improving unimorph piezoelectric vibration energy harvesters based on structural modifications. A new design for a unimorph cantilever-type piezoelectric energy harvester is proposed. The main focus of this paper is to study the resonance frequency and output voltage of the proposed design in piezoelectric mechanical energy harvester and then to increase the bandwidth of the operation of the system.

2- Modal analysis

The structure of unimorph piezoelectric rectangular cantilever is shown in Fig. 1. In Fig. 1, l is the length, w is the width, ρ_s and ρ_p are the substrates and piezoelectric density, t_s and t_p are the substrates and piezoelectric thickness, and E_s and E_p are Young's modulus for substrate and piezoelectric layers, respectively. Also, the total cross-sectional area moment of inertia is \bar{I}_z .

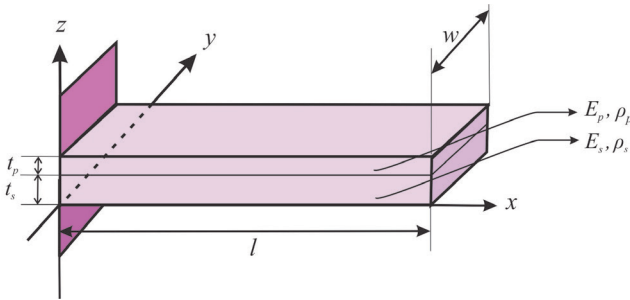


Fig. 1. Schematic of a simple unimorph cantilever beam [6]

For beam cross-sections that are not symmetric about the y-axis about either geometry or the variation of elasticity modulus (E), a convenient method for treating bending problems is provided by the concept of the transformed section. If we choose an absolute value of E as a reference value and call it E_{ref} then we can define a transformed section and transformed width nw , where $n=E_s/E_p$. In this case, we assume that $E_{ref}=E_p$. The line of action of an axial force producing purely axial deformation passes through the centroid of the transformed section. In the case of bending without any axial force, the neutral axis passes through this point. In this case, we assume that the location of the effective centroid is determined by h (Figs. 2 and 3) [29].

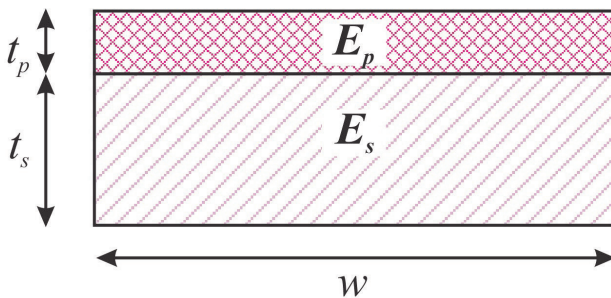


Fig. 2. cross-section of the unimorph cantilever [6]

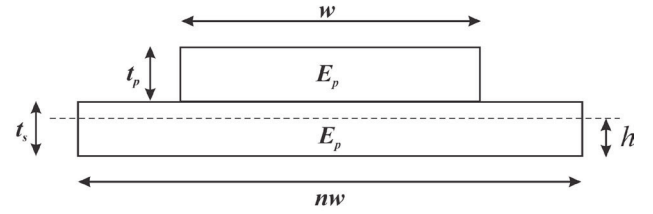


Fig. 3. transformed section of the unimorph cantilever [6]

h is applied for the determination of the neutral axis location:

$$h = \frac{nt_s^2 + 2t_s t_p + t_p^2}{2nt_s + 2t_p} \quad (1)$$

The total cross-sectional area moment of inertia can be expressed as:

$$\bar{I}_z = \frac{nw t_s^3}{12} + n w t_s \left(h - \frac{t_s}{2} \right)^2 + \frac{w t_p^3}{12} + w t_p \left(\frac{t_p}{2} + t_s - h \right)^2 \quad (2)$$

When applying a normal force F at the free end of the cantilever, the deflection function along the length direction can be expressed as:

$$z(x) = \frac{F x^2 (3l - x)}{6 E_p \bar{I}} = K x^2 (3l - x) \quad (3)$$

where K is a constant. The deflection function shown in Eq. (3) can be used as the mode shape, for extracting the resonant behavior of a unimorph cantilever beam with an arbitrary form and width function $w(x)$ [30]. So the vibration displacement at each position is [6]:

$$z(x, \tau) = K x^2 (3l - x) \sin(\omega \tau + \psi) \quad (4)$$

where K and ψ are constants, $\omega = 2\pi f$ is the angular frequency, and τ is the time.

The kinetic energy of the vibrant unimorph cantilever beam can be written as [31]:

$$T = \frac{1}{2} \int_0^l (\rho_s t_s + \rho_p t_p) w(x) dx \left(\frac{\partial z}{\partial \tau} \right)^2 \quad (5)$$

$$= \int_0^l \frac{1}{2} (\rho_s t_s + \rho_p t_p) w(x) [\omega K x^2 (3l - x) \cos(\omega \tau + \alpha)]^2 dx$$

The maximum kinetic energy of the vibrant unimorph cantilever is obtained as [6]:

$$T_{\max} = \frac{1}{2} (\rho_s t_s + \rho_p t_p) \omega^2 K^2 \int_0^l w(x) x^4 (3l - x)^2 dx \quad (6)$$

The potential energy of the system can be written as [31]:

$$V = \frac{1}{2} \iiint_V \sigma_{xx} \epsilon_{xx} dV = \frac{1}{2} \int_0^l \int_{-h}^{+h} \int_{-w/2}^{+w/2} \sigma_{xx} \epsilon_{xx} dV \quad (7)$$

$$= \int_0^l w(x) \left[\frac{\partial z}{\partial x} \right]^2 \left[\frac{E_s}{3} (t_s - h)^3 + \frac{E_s}{3} h^3 + \frac{E_p}{3} (t_s + t_p - h)^3 - \frac{E_p}{3} (t_s - h)^3 \right] dx$$

$$= 18 K^2 \sin^2(\omega \tau + \alpha) \left[\frac{E_s}{3} (t_s - h)^3 + \frac{E_s}{3} h^3 + \frac{E_p}{3} (t_s + t_p - h)^3 - \frac{E_p}{3} (t_s - h)^3 \right] \int_0^l w(x) (l - x)^2 dx$$

So the maximum potential energy of the unimorph cantilever is [6]:

$$V_{\max} = 18K^2 \left[\frac{E_s}{3}(t_s - h)^3 + \frac{E_s}{3}h^3 + \frac{E_p}{3}(t_s + t_p - h)^3 - \frac{E_p}{3}(t_s - h)^3 \right] \times \int_0^l w(x)(l-x)^2 dx \quad (8)$$

According to conservation law of mechanical energy, the resonant frequency can be obtained as:

$$f(w(x)) = \frac{\omega}{2\pi} = \frac{\sqrt{3}}{\pi} \sqrt{\frac{E_s(t_s - h)^3 + E_s h^3 + E_p(t_s + t_p - h)^3 - E_p(t_s - h)^3}{\rho_s t_s + \rho_p t_p}} \times \sqrt{\frac{\int_0^l w(x)(l-x)^2 dx}{\int_0^l w(x)x^4(3l-x)^2 dx}} \quad (9)$$

In the particular case, for a rectangular cantilever with length l_1 , width w_1 , thicknesses t_s and t_p , mass densities ρ_s and ρ_p and Young's modulus E_s and E_p , the deduced resonant frequency is as:

$$f_{\text{rect}} = \frac{\sqrt{385}}{11\pi l_1^2} \sqrt{\frac{E_s(t_s - h)^3 + E_s h^3 + E_p(t_s + t_p - h)^3 - E_p(t_s - h)^3}{\rho_s t_s + \rho_p t_p}} \quad (10)$$

As mentioned in [15], a typical trapezoidal V-shaped cantilever is the result of the difference between one triangular tapered cantilever and one trapezoidal tapered cantilever, with the same thickness, with lengths l_0 and l_1 , and with widths w_0 and w_1 respectively (Fig. 4 (a)). Because of the mirror symmetry of V-shaped cantilever, it is only necessary to analyze half of the geometry, which is a quadrilateral cantilever (Fig. 4 (b)) [6].

Evidently, for the quadrilateral cantilever beam, the width is a piecewise-continuous function of x , that is:

$$w(x) = \begin{cases} \frac{w_1}{2} \left(1 - \frac{x}{l_1 + l_2} \right) - \frac{w_0}{2} \left(1 - \frac{x}{l_0} \right), & x \in [0, l_0] \\ \frac{w_1}{2} \left(1 - \frac{x}{l_1 + l_2} \right), & x \in [l_0, l_1] \end{cases} \quad (11)$$

For simplifying calculations, it is reasonable to define the width ratios a and b , and the length ratio c of the trapezoidal V-shaped cantilever beam:

$$a = \frac{w_2}{w_1}, b = \frac{w_0}{w_1}, c = \frac{l_0}{l_1} \quad (12)$$

By Substituting Eqs. (11) and (12) into Eq. (9), the resonant frequency formula of the trapezoidal cantilever beam is obtained [6]:

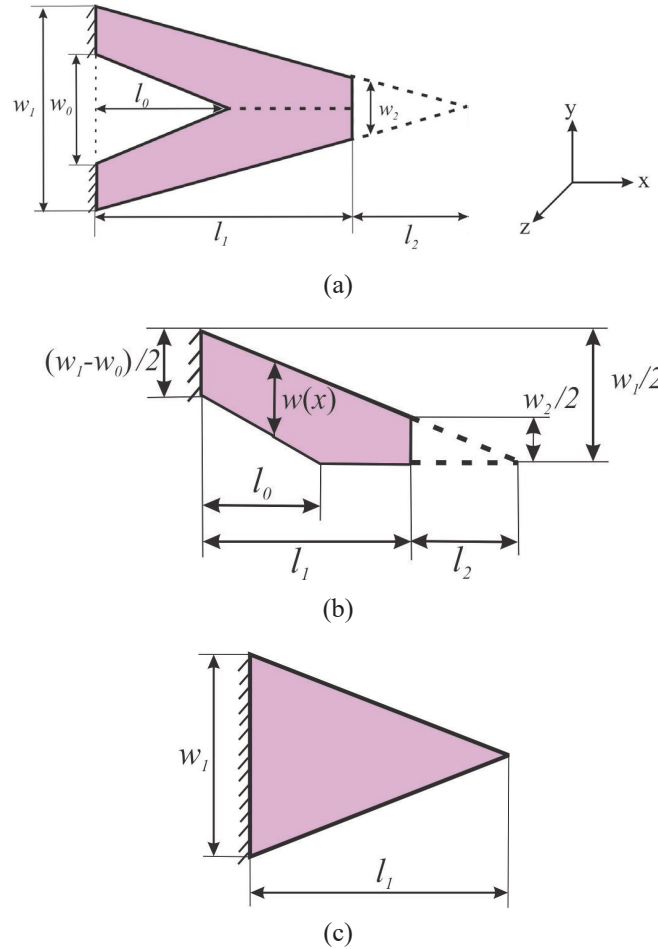


Fig. 4. Shape and dimension of (a) trapezoidal V-shaped cantilever beam (b) half of the trapezoidal V-shaped cantilever beam (c) triangular tapered cantilever beam [6]

$$f(w(x)) = \frac{\sqrt{70}}{\pi l_1^2} \sqrt{\frac{E_s(t_s - h)^3 + E_s h^3 + E_p(t_s + t_p - h)^3 - E_p(t_s - h)^3}{\rho_s t_s + \rho_p t_p}} \times \sqrt{\frac{3 + a - 6bc + 4bc^2 - bc^3}{49 + 250a - 84bc^5 + 40bc^6 - 5bc^7}} \quad (13)$$

In order to represent the relationship between the resonant frequency and the ratios a , b and c , a characteristic function regarding a , b and c can be defined as mentioned in [15,27]

$$g(a,b,c) = \sqrt{\frac{3 + a - 6bc + 4bc^2 - bc^3}{49 + 250a - 84bc^5 + 40bc^6 - 5bc^7}} \quad (14)$$

$a \in [0, 1], b \in [0, 1], c \in [0, 1]$

Hence, the resonant frequency of unimorph trapezoidal V-shaped cantilever beam is:

$$f(w(x)) = \frac{\sqrt{70}}{\pi l_1^2} \sqrt{\frac{E_s(t_s - h)^3 + E_s h^3 + E_p(t_s + t_p - h)^3 - E_p(t_s - h)^3}{\rho_s t_s + \rho_p t_p}} g(a,b,c) \quad (15)$$

For a unimorph triangular tapered cantilever, $a=0$ and the

resonant frequency is:

$$f(w(x)) = \frac{\sqrt{70}}{\pi l_1^2} \sqrt{\frac{E_s(t_s - h)^3 + E_s h^3 + E_p(t_s + t_p - h)^3 - E_p(t_s - h)^3}{\rho_s t_s + \rho_p t_p}} g(a=0, b, c) \quad (16)$$

In other words, characteristic function will be summarized as:

$$g(b, c) = \sqrt{\frac{3 - 6bc + 4bc^2 - bc^3}{49 - 84bc^5 + 40bc^6 - 5bc^7}} \quad (17)$$

$b \in [0, 1], c \in [0, 1]$

In the particular case that $t_p=0$ and $a=0$, the resonant frequency formulation for a simple triangular cantilever beam is obtained that is by that extracted in [28].

As shown in Fig. 5, $g(a, b, c)$ reaches the maximum value $(\sqrt{3}/7) \approx 0.2474$, when $a=0$ and $c=0$ or $c=1$ or $b=0$. That means if $l_0=0$ or $l_0=l_2$ or $w_0=0$, unimorph trapezoidal V-shaped cantilever achieves highest resonant frequency. For $w_2=0$ and $l_0=0$ or $w_0=0$, the unimorph trapezoidal V-shaped cantilever beam turns into a unimorph triangular tapered cantilever beam as shown in Fig. 4 (c). When $w_2=0$ and $l_0=l_1$, the unimorph V-shaped cantilever turns into two side by side unimorph tapered cantilever beams, though, this particular uncommon form is difficult to accomplish. Therefore, unimorph tapered cantilever beam that is easy for micro-fabrication and is a special kind of unimorph V-shaped cantilever beam can reach the maximum resonant frequency. In other words, it has the highest sensitivity. It is notable that the behavior of $g(a, b, c)$ in Fig. 5 is such as that obtained in [6, 32].

3- The potential electrical response of a unimorph piezoelectric cantilever

Because of the low thickness of the beam, Euler-Bernoulli theory is considered in deriving the mathematical modeling of the structure. The governing equation of motion for a beam embedded by a single piezoelectric layer under the influence of base excitation is as follows [33]:

$$\frac{\partial^2 M(x, t)}{\partial x^2} + \frac{\partial^2}{\partial x^2} \left(C_s I(x) \frac{\partial^3 z(x, t)}{\partial x^2 \partial t} \right) + C_a \frac{\partial z(x, t)}{\partial t} + m(x) \frac{\partial^2 z(x, t)}{\partial t^2} = -[m(x) + M_t \delta(x - L)] \frac{\partial^2 z_b(x, t)}{\partial t^2} \quad (18)$$

where $M(x, t)$ is the internal moment, $z(x, t)$ is the transverse displacement of the neutral axis, $z_b(x, t)$ is the base excitation displacement, C_s and C_a are equivalent strain rate and viscous air damping coefficient, $I(x)$ is the area moment of inertia, $m(x)$ is the mass per unit length of the beam, and M_t is the tip mass. For this structure, the boundary conditions of the system are described in Eq. (19), i.e., the cantilever is fixed at $x=0$ and attached to a tip mass at the other end [19].

$$z(0, t) = 0, \frac{\partial z(x, t)}{\partial x} = 0, EI \frac{\partial^3 z(x, t)}{\partial x^3} = M_t \frac{\partial^2 z(x, t)}{\partial t^2}, EI \frac{\partial^2 z(x, t)}{\partial x^2} = I_t \frac{\partial^3 z(x, t)}{\partial x \partial t^2} \quad (19)$$

where I_t is the rotary inertia of the tip mass. Here it is assumed to neglect the tip mass.

As the unimorph cantilever, consists of two layers with different materials, m can be written as:

$$m = w(\rho_s t_s + \rho_p t_p) \quad (20)$$

where w is the width, t is the thickness and ρ is the density. Also, the subscripts s and p , are for substrate and piezoelectric layers, respectively. Here, the width of the piezoelectric layer is assumed to be the same as the width of the substrate layer, denoted by w . The internal moment $M(x, t)$, can be written as [6]:

$$M(x, t) = -\int_{-(t_s/2)}^{(t_s/2)} \sigma_1^s w y dy - \int_{(t_s/2)}^{(t_s/2)+t_p} \sigma_1^p w y dy \quad (21)$$

By using the constitutive equation of piezoelectric and

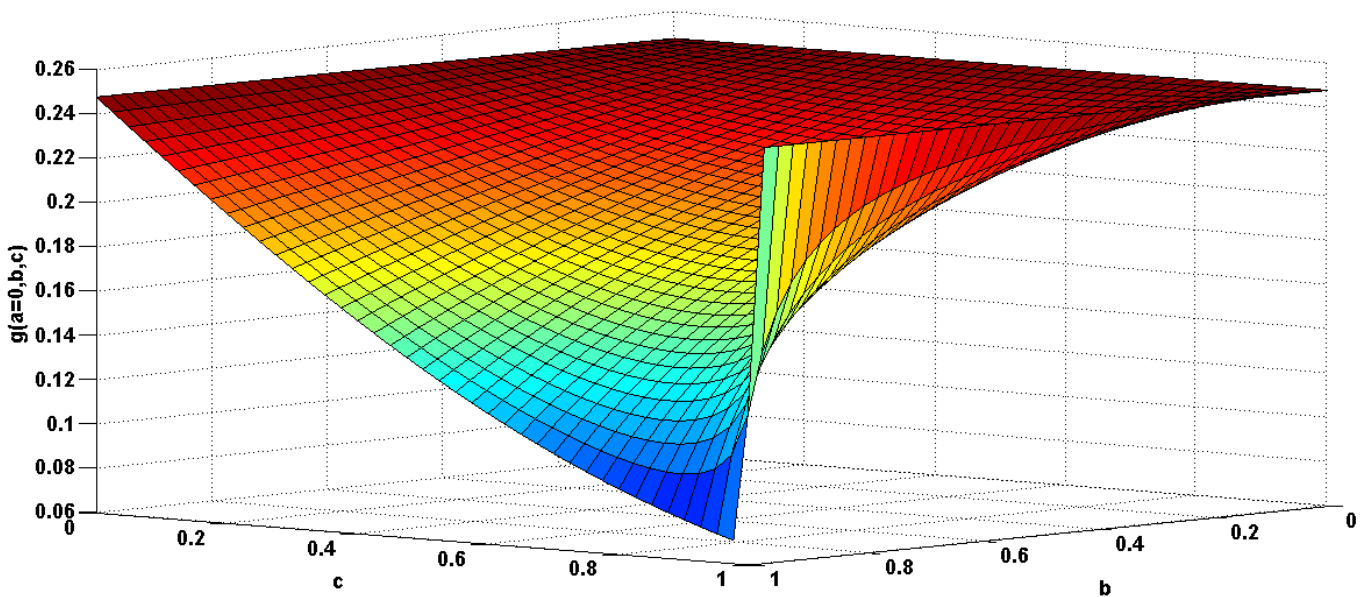


Fig. 5. The function image of $g(a=0, b, c)$ [6]

isotropic material, the stress terms in Eq. (21) can be written as follows:

$$\sigma_1^s = E_s \varepsilon_1^s(x, t) \quad (22)$$

$$\sigma_1^p = E_p (\varepsilon_1^p(x, t) - d_{31} E_3(t)) \quad (23)$$

where σ is the normal stress in the x -direction, ε is the mechanical strain, d_{31} is the piezoelectric strain constant, and E_3 is the applied electrical field. E_3 can be written regarding voltage $v(t)$ as below [6]:

$$E_3(t) = -v(t) / h_p \quad (24)$$

The bending strain, ε at any level, z from the neutral axis can be expressed as below:

$$\varepsilon_1 = -y \frac{\partial^2 z_{rel}(x, t)}{\partial x^2} \quad (25)$$

Employing Eqs. (22) to (23) and (25) into Eq. (21), one may obtain:

$$M(x, t) = EI(x) \frac{\partial^2 z_{rel}(x, t)}{\partial x^2} + \eta(x) v(t) \quad (26)$$

where:

$$\eta(x) = -\frac{1}{2} E_p w(x) d_{31} (t_p + t_s) \quad (27)$$

Using Heaviside step function, the internal moment can be written as:

$$M(x, t) = EI(x) \frac{\partial^2 z_{rel}(x, t)}{\partial x^2} + \eta(x) v(t) [He(x) - He(x - l)] \quad (28)$$

where l is the length of the beam, and the piezoelectric layer covers all of this length. Employing Eq. (28) into Eq. (18) yields:

$$\begin{aligned} & \frac{\partial^2}{\partial x^2} \left[EI(x) \frac{\partial^2 z_{rel}(x, t)}{\partial x^2} \right] + \frac{\partial^2}{\partial x^2} \left[C_s I(x) \frac{\partial^3 z_{rel}(x, t)}{\partial x^2 \partial t} \right] \\ & + C_a \frac{\partial z_{rel}(x, t)}{\partial t} + m(x) \frac{\partial^2 z_{rel}(x, t)}{\partial t^2} \\ & + \frac{\partial^2}{\partial x^2} \left[\eta(x) v(t) \left[\frac{d\delta(x)}{dx} - \frac{d\delta(x-l)}{dx} \right] \right] = \\ & -(m(x) + M_t \delta(x-l)) \frac{\partial^2 z_b(x, t)}{\partial t^2} \end{aligned} \quad (29)$$

The constitutive equation of piezoelectric materials that relates the electrical and mechanical terms is given by:

$$D_3(x, t) = d_{31} \sigma_1(x, t) + \varepsilon_{33}^T E_3(t) \quad (30)$$

Here $D_3(x, t)$ is the electrical displacement, $\sigma_1(x, t)$ is the normal stress in the x -direction and ε_{33}^T is the permittivity at constant

stress. The permittivity at constant strain ε_{33}^S replaces the permittivity component through $\varepsilon_{33}^S = \varepsilon_{33}^T - d_{31} E_3$. Thus Eq. (30) can be rewritten as [6]:

$$D_3(x, t) = -d_{31} E_p \left(\frac{t_s}{2} + t_p \right) \frac{\partial^2 z_{rel}(x, t)}{\partial x^2} - \varepsilon_{33}^S \frac{v(t)}{t_p} \quad (31)$$

Integrating the electrical displacement over the piezoelectric area leads to generated electric charge in the piezoelectric layer, $q(t)$, as below:

$$q(t) = \int \vec{D}_3 \cdot \vec{n} dA = - \int_{x=0}^{x=l} \left(d_{31} \left(\frac{t_s}{2} + t_p \right) E_p w(x) \frac{\partial^2 z_{rel}(x, t)}{\partial x^2} + \varepsilon_{33}^S w(x) \frac{v(t)}{t_p} \right) dx \quad (32)$$

where \vec{n} is unit outward standard and \vec{D} is the vector of electric displacement. Value of the current, $i(t)$ is obtained by differentiating electrical charge over time. Therefore, the voltage across the resistive load can be obtained as follows:

$$v(t) = R_L i(t) = -R_L \left[\int_{x=0}^{x=l} \left(d_{31} \left(\frac{t_s}{2} + t_p \right) E_p w(x) \frac{\partial^3 z_{rel}(x, t)}{\partial x^2 \partial t} \right) dx + \frac{\varepsilon_{33}^S w(x) l}{t_p} \frac{dv(t)}{dt} \right] \quad (33)$$

Rearranging the Eq. (33) leads to:

$$\begin{aligned} & \frac{dv(t)}{dt} + \frac{t_p}{\varepsilon_{33}^S w(x) l R_L} v(t) = \\ & - \frac{d_{31} \left(\frac{t_s}{2} + t_p \right) E_p t_p}{\varepsilon_{33}^S l} \int_{x=0}^{x=l} \frac{\partial^3 z_{rel}(x, t)}{\partial x^2 \partial t} dx \end{aligned} \quad (34)$$

Using the separation of variables technique leads to [6]:

$$z_{rel}(x, t) = \sum_{k=1}^{\infty} w_k(x) q_k(t) \quad (35)$$

Using Eq. (35), the integral term in Eq. (34) can be written as:

$$\begin{aligned} & \int_{x=0}^{x=l} \frac{\partial^3 z_{rel}(x, t)}{\partial x^2 \partial t} dx = \\ & \sum_{k=1}^{\infty} \frac{dq_k(t)}{dt} \int_0^l \frac{d^2 w_k(x)}{dx^2} dx = \frac{dq_k(t)}{dt} \frac{dw_k(x)}{dx} \Big|_{x=l} \end{aligned} \quad (36)$$

By simplifying Eq. (34) the ordinary differential equation of piezoelectric energy harvester will be as follows:

$$\frac{dv(t)}{dt} + \frac{t_p}{\varepsilon_{33}^S w l R_L} v(t) = \sum_{k=1}^{\infty} \phi_k \frac{dq_k(t)}{d\tau} \quad (37)$$

where:

$$\phi_k(x) = - \frac{d_{31} E_p h_p (h_s / 2 + h_p)}{\varepsilon_{33}^S L} \frac{dw_k(x)}{dx} \Big|_{x=l} \quad (38)$$

Eq. (37) can be solved for $v(t)$ by multiplying the following integrating factor through the differential equation in order to

bring the left-hand side under a common derivative:

$$\psi(t) = e^{\tau/\tau_c} \quad (39)$$

where τ_c is the circuit time constant and can be expressed by:

$$\tau_c = \frac{R_L \epsilon_{33}^s W l}{t_p} \quad (40)$$

Combining Eqs. (29) and (35) leads to:

$$\begin{aligned} & \sum_{k=1}^{\infty} \frac{d^2}{dx^2} \left[EI(x) \frac{d^2 w_k(x)}{dx^2} \right] q_k(t) \\ & + \sum_{k=1}^{\infty} \left\{ \frac{d^2}{dx^2} \left[C_s I(x) \frac{d^2 w_k(x)}{dx^2} \right] + C_a \right\} \frac{dq_k(t)}{dt} \\ & + m(x) \sum_{k=1}^{\infty} w_k(x) \frac{d^2 q_k(t)}{dt^2} \\ & + \frac{d^2}{dx^2} \left[\eta(x) \left[\frac{d\delta(x)}{dx} - \frac{d\delta(x-l)}{dx} \right] \right] v(t) = \\ & - [m(x) + M_i \delta(x-l)] \frac{\partial^2 z_b(x,t)}{\partial t^2} \end{aligned} \quad (41)$$

Integrating Eq. (41) over the length of the beam after multiplying it by $w_k(x)$ and using orthogonality condition gives the equation of motion as follows:

$$\begin{aligned} & \frac{d^2 q_k(\tau)}{d\tau^2} + 2\zeta_k \omega_k \frac{dq_k(\tau)}{d\tau} + \omega_k^2 q_k(\tau) + \lambda_k v(\tau) = \\ & - \left[\int_0^l w_k(x) m(x) dx + M_i w_k(l) \right] \frac{d^2 w_b(x)}{dt^2} \end{aligned} \quad (42)$$

where λ_k represents the modal coupling term and is dependent on the cantilever shape. For a rectangular cantilever it can be obtained as:

$$\lambda_k = \eta \left. \frac{dw_k(x)}{dx} \right|_{x=l} \quad (43)$$

For an exponentially tapered cantilever, the modal coupling term is expressed as below:

$$\begin{aligned} \lambda_k = & \int_0^l w_k(x) \frac{d^2 \eta(x)}{dx^2} dx + \left. \frac{d(w_k(x)\eta(x))}{dx} \right|_{x=0} \\ & - \left. \frac{d(w_k(x)\eta(x))}{dx} \right|_{x=l} + 2 \left(w_k(0) \frac{d\eta(x)}{dx} \right)_{x=0} - w_k(l) \frac{d\eta(x)}{dx} \Big|_{x=l} \end{aligned} \quad (44)$$

Modal damping ratio can be estimated using half power bandwidth method or based on the motion decay in viscous damping. If beam oscillation is harmonic in time, base motion, output voltage, and electrical charge can be written as $z_b = Y_0 e^{i\omega t}$, $v(t) = V_0 e^{i\omega t}$ and $q_k(t) = Q_k e^{i\omega t}$ respectively. Thus $q_k(t)$ becomes:

$$q_k(t) = \frac{\left[m\omega^2 Y_0 \int_0^l w_k(x) dx - \lambda_k V_0 \right] e^{i\omega t}}{\omega_k^2 - \omega^2 + 2i\zeta_k \omega_k \omega} \quad (45)$$

where i is the imaginary number sign and ω is the driving frequency. Also substituting $v(t) = V_0 e^{i\omega t}$ in Eq. (37) can lead to:

$$\left(\frac{1 + i\omega\tau_c}{\tau_c} \right) V_0 e^{i\omega t} = \sum_{k=1}^{\infty} \phi_k \frac{dq_k(t)}{dt} \quad (46)$$

Differentiating Eq. (45) and substituting in Eq. (46) can lead to the voltage amplitude across the resistance:

$$\begin{aligned} & \left(\frac{1 + i\omega\tau_c}{\tau_c} \right) V_0 e^{i\omega t} = \\ & \sum_{k=1}^{\infty} \phi_k \frac{i\omega \left[m\omega^2 Y_0 \int_0^l w_k(x) dx - \lambda_k V_0 \right] e^{i\omega t}}{\omega_k^2 - \omega^2 + 2i\zeta_k \omega_k \omega} \end{aligned} \quad (47)$$

So the ratio of the output voltage to the base acceleration or voltage Frequency Response Function (FRF) is as below:

$$\frac{v(t)}{\omega^2 Y_0 e^{i\omega t}} = \frac{\sum_{k=1}^{\infty} \frac{im\omega\phi_k \left(\int_0^l w_k(x) dx \right)}{\omega_k^2 - \omega^2 + 2i\zeta_k \omega_k \omega}}{\left(\sum_{k=1}^{\infty} \frac{i\omega\lambda_k\phi_k}{\omega_k^2 - \omega^2 + 2i\zeta_k \omega_k \omega} \right) + \frac{1 + i\omega\tau_c}{\tau_c}} \quad (48)$$

For a series connection of cantilever beams, the output voltage is deduced as:

$$\frac{v(t)}{\omega^2 Y_0 e^{i\omega t}} \Big|_{\text{series-connection}} = \sum_{n=1}^{n_0} \frac{\sum_{k=1}^{\infty} \frac{im\omega\phi_k \left(\int_0^l w_k(x) dx \right)}{\omega_k^2 - \omega^2 + 2i\zeta_k \omega_k \omega}}{\left(\sum_{k=1}^{\infty} \frac{i\omega\lambda_k\phi_k}{\omega_k^2 - \omega^2 + 2i\zeta_k \omega_k \omega} \right) + \frac{1 + i\omega\tau_c}{\tau_c}} \quad (49)$$

where n_0 is the number of cantilevers.

Similar equations can be used for series connection of triangular cantilever energy harvesters using pizza scheme (Fig. 6). The proposed layout is similar to the pizza slices, except that the slices have triangular geometry. The pizza scheme takes up very little space and produces more power than the conventional layouts.

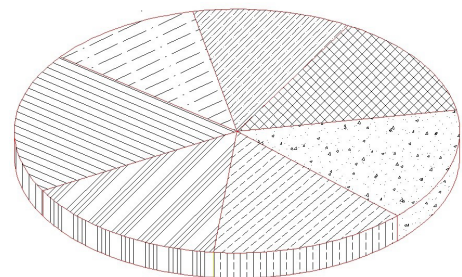


Fig. 6. Pizza layout of the cantilever energy harvesters

It is notable that for tapered cantilevers, some modifications in the area moment of inertia, $I(x)$, and the width function, $w(x)$, must be considered. In this case, the width function of beam shape is defined as [25]:

$$w(x) = (ratio \times w(0)) + \frac{w(0)(1 - ratio)}{l}(l - x) \quad (50)$$

4- Experiment setup

The samples are manufactured using the Aluminum substrate and PZT-5H as the piezoelectric layer. The wires are soldered to the piezoelectric layer in approximately 285 °C (Fig. 7). The solder time should not exceed 2–3 seconds, in order to minimize the heat transfer to the piezoelectric layer and thus decrease the risk of the depolarization of the piezoceramic material. There are some critical points in the soldering procedure that is mentioned in [15].



Fig. 7. Soldering the wires to the piezoelectric layer

After bonding the layers, the cantilever is fixed into the designed fixture and are put into the shaker (Fig. 8) [34]. The piezoceramic is brittle, and the necessary attention must be paid. The schematic diagram for the experimental study is shown in Fig. 9. One rectangular and three triangular specimens are manufactured for test and analysis.



Fig. 8. Cantilever energy harvester that is mounted on the shaker

5- Experimental Results and analysis

For verification of the results, experimental work is done for rectangular and triangular geometries. For a rectangular cantilever, the analytical and experimental results are shown in Figs. 10 and 11. As can be seen, there is a good agreement between the experimental and theoretical results. A similar comparison is done for three different triangular cantilevers with different thicknesses of the substrate layers.

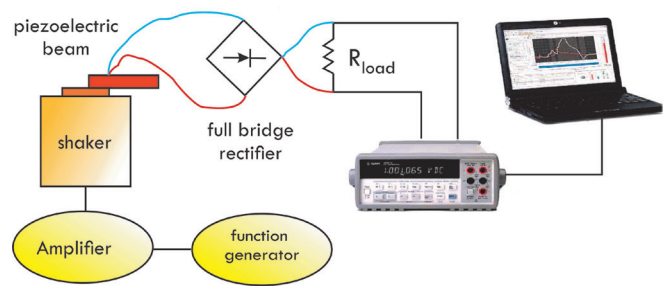


Fig. 9. Schematic diagram of the experimental setup

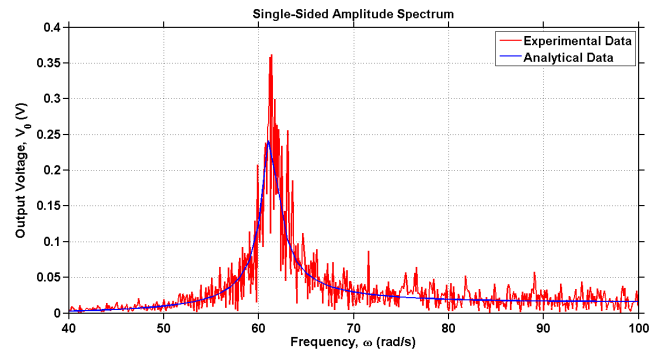


Fig. 10. Comparison of the experimental and analytical results for the rectangular cantilever energy harvester

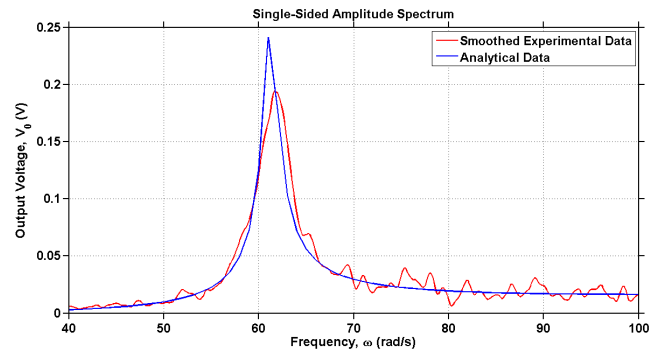


Fig. 11. Comparison of the experimental and analytical results for the rectangular cantilever energy harvester using smoothed experimental data

A pizza layout energy harvesting system can be used for showing the triangular cantilevers. The thickness of the substrate layers for three cantilevers (P1, P2, and P3) are 0.28, 0.30 and 0.33 mm, respectively. The length of the rectangular and triangular cantilevers are equal to 7.24 cm. Also, the width of the cantilevers in the base is similar to each other and equal to 1.72 cm. The results for the first triangular sample are shown in Figs. 12 and 13. The results for the second triangular sample are shown in Figs. 14 and 15, and the results for the third sample are shown in Figs. 16 and 17. As can be seen, there is a good agreement between the experimental and theoretical results for both of the resonance frequency and output voltage. For a better comparison, the smoothed data are shown. The notable point is that there are many smoothing algorithms, and using different algorithms leads to different results. So the most accurate comparison can be obtained using the actual data. However, using smoothed experimental data gives a better overview.

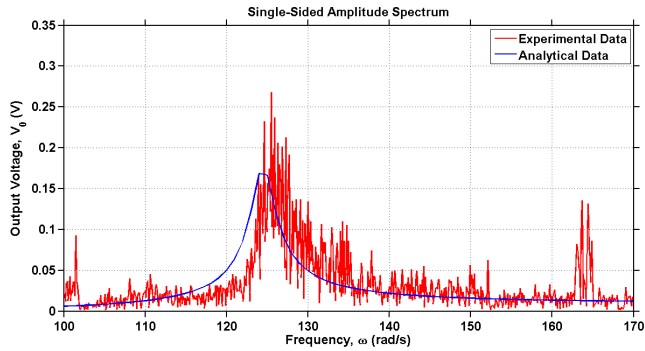


Fig. 12. Comparison of the experimental and analytical results for the 1st triangular cantilever energy harvester (P1)

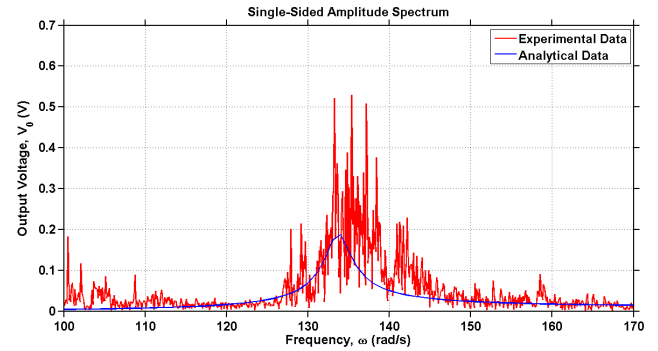


Fig. 16. Comparison of the experimental and analytical results for the 3rd triangular cantilever energy harvester (P3)

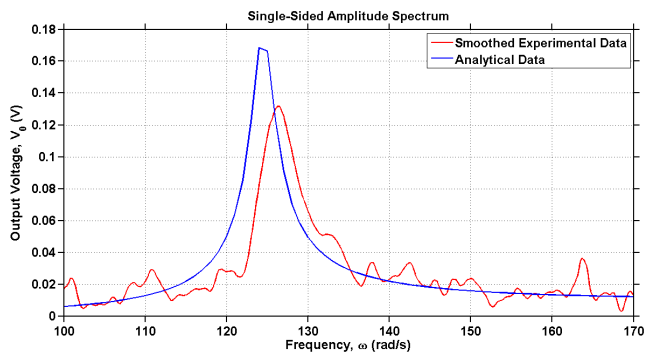


Fig. 13. Comparison of the experimental and analytical results for the 1st triangular cantilever energy harvester (P1) using smoothed experimental data

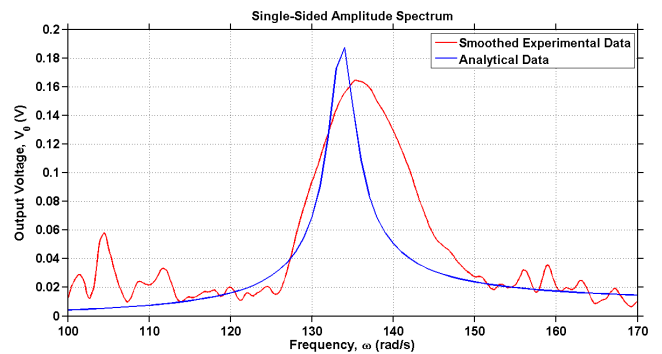


Fig. 17. Comparison of the experimental and analytical results for the 3rd triangular cantilever energy harvester (P3) using smoothed experimental data

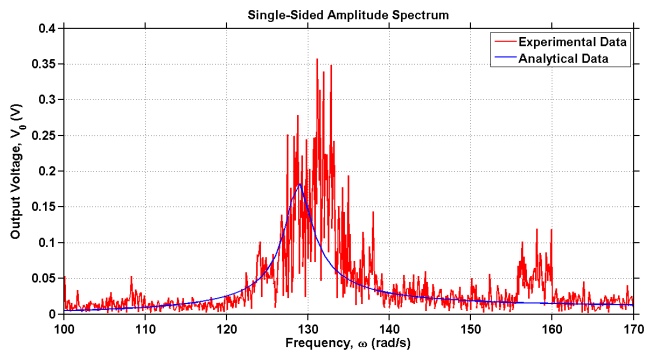


Fig. 14. Comparison of the experimental and analytical results for the 2nd triangular cantilever energy harvester (P2)

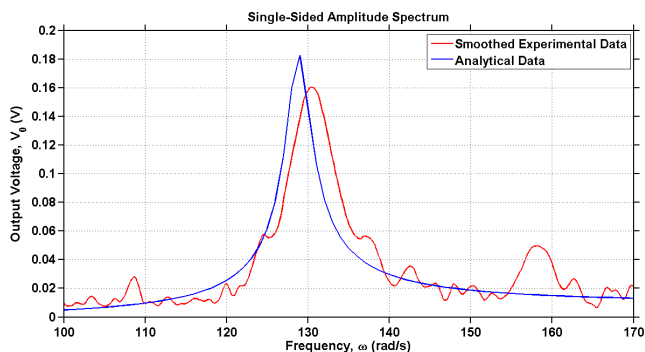


Fig. 15. Comparison of the experimental and analytical results for the 2nd triangular cantilever energy harvester (P2) using smoothed experimental data

The peak of the output voltage (experimentally and analytically) are mentioned in Table 1. As can be seen, the maximum relative error is less than 21.4%. The relative error can be due to human and equipment errors. However, since the theoretical values are less than the experimental ones, one of the essential parts of the errors may be due to energy loss.

Table 1. Maximum experimental and analytical output voltage and the relative error (%)

	1 st sample (P1)	2 nd sample (P2)	3 rd sample (P3)
Experimental maximum output voltage	0.132	0.160	0.164
Analytical maximum output voltage	0.168	0.183	0.187
Relative error (%)	21.4	12.6	12.3

For widening the bandwidth of the energy harvester structure, the triangular cantilevers are connected with a series connection. As can be expected, the output voltages are added together. For a comparison between the output of the separated cantilevers and the connected one, the voltages of cantilever energy harvesters are added together and plotted with the connected structure. The results are shown in Fig. 18, and the relative error is less than 6%. Multiple cantilevers or cantilever arrays integrated into one energy harvesting device (a pizza form energy harvester) can easily achieve continuous wide bandwidth if the geometric parameters of the harvester are appropriately selected [35]. Using a cantilever array method, some close modes and thus more full bandwidth could be achieved as compared

to a single-beam harvester that its operation bandwidth is usually narrow. Both the bandwidth and the voltage peaks are increased by using the cantilever array method, and using pizza form can decrease the volume of the energy harvester. The three voltage peaks are coupled together in the 3-Degree-Of-Freedom (DOF) harvester to form a relatively broad bandwidth. The bandwidth of each cantilever alone is about 4.1 Hz, 4.8 Hz, and 9.7 Hz, respectively. The three modes could be designed to be very close to each other, and 443% increase in bandwidth (bandwidth is 22.3 Hz) at a voltage level of 0.1 V was achieved as compared to a conventional Single Degree-Of-Freedom (SDOF) device in the experiment (first triangular cantilever).

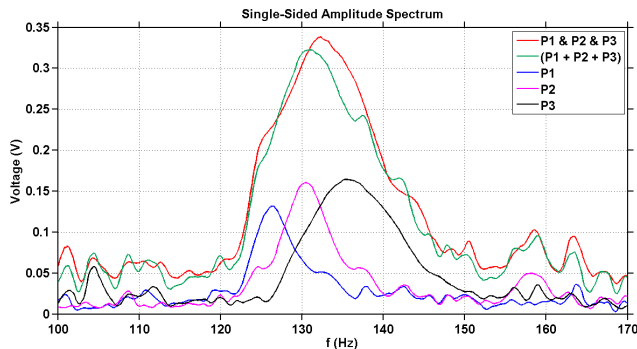


Fig. 18. Comparison of the experimental and analytical results for the series connection of the triangular cantilever energy harvesters

6- Conclusion

This paper deduces a highly precise explicit formula for approximating the fundamental resonant frequency of unimorph trapezoidal V-shaped cantilevers based on the Rayleigh-Ritz method. The analytical results are in a good agreement with the experimental results, and the relative error is negligible. In addition to determining the resonant frequency of unimorph trapezoidal V-shaped cantilevers of any material and geometrical properties, the presented resonant frequency formula can be used for design and optimization of unimorph trapezoidal V-shaped cantilever energy harvesters which are considered among the best and highest performance. The shape of the cantilever in the first mode of vibration is not precisely the same as the static deflection profile. So the natural frequency estimates are slightly different from the simulation values. The formula presented for calculating natural frequency of unimorph tapered cantilevers is a simple, relatively precise and practical formula for providing design guidelines. Also, the output voltage of the unimorph piezoelectric cantilever beam is formulated, and the formula is validated by experimental results. Experimental results demonstrate that under the same loading, material and geometrical conditions, triangular cantilever beams are more efficient than rectangular ones. It turns out that the shape can have a significant effect on the output voltage and therefore maximum output power density. Combining the triangular shape energy harvesters and multi-modal energy harvester design, can provide the highest power density and consequently optimized design schemes. The base of the design is to closing the resonance frequencies of the cantilever array to create a wideband energy harvester system. Because of the unique phenomenon, the proposed

harvester is shown to be very useful in broadening the operation bandwidth with three adjacent voltage peaks. The results of this study can provide design guidance toward fabricating high power and wideband piezoelectric energy harvesters.

References

- [1] M.R. Forouzan, R. Hoseini, Dynamic Analysis of a Modified Truck Chassis, *International Journal of Advanced Design and Manufacturing Technology*, 3(4) (2010) 31-36.
- [2] R. Hoseini, H. Salehipour, Investigation into the Importance of Pre-Design Procedure in Vibration Absorbers Installations, *International Journal of Advanced Design and Manufacturing Technology*, 4(1) (2011) 55-62.
- [3] R. Hosseini, H. Salehipoor, Optimum design process of vibration absorber via imperialist competitive algorithm, *International Journal of Structural Stability and Dynamics*, 12(03) (2012) 1250019.
- [4] R. Hosseini, K. Firoozbakhsh, H. Naseri, Optimal design of a vibration absorber for tremor control of arm in Parkinson's disease, *Journal of Computational and Applied Research in Mechanical Engineering (JCARME)*, 3(2) (2014) 85-94.
- [5] H. Salehipour, R. Hosseini, K. Firoozbakhsh, Exact 3-D solution for free bending vibration of thick FG plates and homogeneous plate coated by a single FG layer on elastic foundations, *Journal of Solid Mechanics*, 7(1) (2015) 28-40.
- [6] R. Hosseini, M. Nouri, Shape design optimization of unimorph piezoelectric cantilever energy harvester, *Journal of Computational Applied Mechanics*, 47(2) (2016) 247-259.
- [7] R. Hosseini, M. Hamed, A. Ebrahimi Mamaghani, H.C. Kim, J. Kim, J. Dayou, Parameter identification of partially covered piezoelectric cantilever power scavenger based on the coupled distributed parameter solution, *International Journal of Smart and Nano Materials*, 8(2-3) (2017) 110-124.
- [8] R. Hosseini, M. Hamed, J. Im, J. Kim, J. Dayou, Analytical and experimental investigation of partially covered piezoelectric cantilever energy harvester, *International Journal of Precision Engineering and Manufacturing*, 18(3) (2017) 415-424.
- [9] B. Shahriari, O. Zargar, M. Baghani, M. Baniassadi, Free vibration analysis of rotating functionally graded annular disc of variable thickness using generalized differential quadrature method, *Scientia Iranica*, 25(2) (2018) 728-740.
- [10] M. Mohammadsalehi, O. Zargar, M. Baghani, Study of non-uniform viscoelastic nanoplates vibration based on nonlocal first-order shear deformation theory, *Meccanica*, 52(4-5) (2017) 1063-1077.
- [11] R. Hosseini, O. Zargar, M. Hamed, Improving Power Density of Piezoelectric Vibration-Based Energy Scavengers, *Journal of Solid Mechanics Vol*, 10(1) (2018) 98-109.
- [12] S. Priya, D.J. Inman, *Energy harvesting technologies*,

- Springer, 2009.
- [13] N. Elvin, A. Erturk, *Advances in energy harvesting methods*, Springer Science & Business Media, 2013.
- [14] S. Beeby, N. White, *Energy harvesting for autonomous systems*, Artech House, 2014.
- [15] R. Hosseini, M. Hamed, Improvements in energy harvesting capabilities by using different shapes of piezoelectric bimorphs, *Journal of Micromechanics and Microengineering*, 25(12) (2015).
- [16] R. Hosseini, M. Hamed, Study of the resonant frequency of unimorph triangular V-shaped piezoelectric cantilever energy harvester, *International Journal of Advanced Design and Manufacturing Technology*, 8(4) (2015).
- [17] J. Baker, S. Roundy, P. Wright, Alternative geometries for increasing power density in vibration energy scavenging for wireless sensor networks, in: *Proceedings of the Third International Energy Conversion Engineering Conference*, San Francisco, 2005.
- [18] M.H. Jalali, O. Zargar, M. Baghani, Size-Dependent Vibration Analysis of FG Microbeams in Thermal Environment Based on Modified Couple Stress Theory, *Iranian Journal of Science and Technology, Transactions of Mechanical Engineering*, (2018) 1-11.
- [19] A.D. Dimarogonas, *Vibration for engineers*, Prentice Hall, 1996.
- [20] T.A. Anderson, D.W. Sexton, A vibration energy harvesting sensor platform for increased industrial efficiency, in: *Smart structures and materials, International Society for Optics and Photonics*, 2006, pp. 61741Y-61741Y-61749.
- [21] S.P. Beeby, M.J. Tudor, N. White, Energy harvesting vibration sources for microsystems applications, *Measurement science and technology*, 17(12) (2006) R175.
- [22] A. Erturk, D.J. Inman, A distributed parameter electromechanical model for cantilevered piezoelectric energy harvesters, *Journal of vibration and acoustics*, 130(4) (2008) 041002.
- [23] S. Matova, M. Renaud, M. Jambunathan, M. Goedbloed, R. Van Schaijk, Effect of length/width ratio of tapered beams on the performance of piezoelectric energy harvesters, *Smart Materials and Structures*, 22(7) (2013) 075015.
- [24] N. Siddiqui, *Understanding effects of tapering cantilevered piezoelectric bimorph for energy harvesting from vibrations*, PhD thesis, Auburn University, 2014.
- [25] A.G. Muthalif, N.D. Nordin, Optimal piezoelectric beam shape for single and broadband vibration energy harvesting: Modeling, simulation and experimental results, *Mechanical Systems and Signal Processing*, 54 (2015) 417-426.
- [26] R. Hosseini, M. Hamed, An investigation into resonant frequency of trapezoidal V-shaped cantilever piezoelectric energy harvester, *Microsystem Technologies*, 22(5) (2016) 1127-1134.
- [27] R. Hosseini, M. Hamed, An Investigation into Resonant Frequency of Triangular V-Shaped Cantilever Piezoelectric Vibration Energy Harvester, *Journal of Solid Mechanics*, 8(3) (2016) 560-567.
- [28] K. Yang, Z. Li, Y. Jing, D. Chen, T. Ye, Research on the resonant frequency formula of V-shaped cantilevers, in: *2009 4th IEEE International Conference on Nano/Micro Engineered and Molecular Systems*, 2009, pp. 59-62.
- [29] J. Lubliner, P. Papadopoulos, *Introduction to solid mechanics: an integrated approach*, Springer Science & Business Media, 2013.
- [30] C.W. De Silva, *Vibration: fundamentals and practice*, CRC press, 2006.
- [31] S.S. Rao, *Vibration of continuous systems*, John Wiley & Sons, 2007.
- [32] R. Hosseini, M. Hamed, Resonant frequency of bimorph triangular V-shaped piezoelectric cantilever energy harvester, *Journal of Computational & Applied Research in Mechanical Engineering (JCARME)*, 6(1) (2016) 65-73.
- [33] A. Erturk, D.J. Inman, *Piezoelectric energy harvesting*, John Wiley & Sons, 2011.
- [34] O. Zargar, A. Masoumi, A.O. Moghaddam, Investigation and optimization for the dynamical behaviour of the vehicle structure, *International Journal of Automotive and Mechanical Engineering*, 14 (2017) 4196-4210.
- [35] L. Tang, Y. Yang, C.K. Soh, *Broadband vibration energy harvesting techniques*, in: *Advances in energy harvesting methods*, Springer, 2013, pp. 17-61.

Please cite this article using:

R. Hosseini, M. Hamed, H. Golparvar, O. Zargar, Analytical and Experimental Investigation into Increasing Operating Bandwidth of Piezoelectric Energy Harvesters, *AUT J. Mech. Eng.*, 3(1) (2019) 113-122.

DOI: 10.22060/ajme.2018.14272.5718

